Supplementary Information

Unveiling the Sensing Ability of MoS_2 Nanoparticles: from Fundamental Insights into Practical Applications for Nitrites

Federica Florio, [a] Angelo Ferlazzo, [a] Stefano Bonforte, [a] Giuseppe Nicotra, [b] Giovanni Neri, [c] Iddo Pinkas, [d] Milko E. van der Boom [e]*, and Antonino Gulino [a]*

[a] *Department of Chemical Sciences, University of Catania, and I.N.S.T.M. U.d.R. of Catania, Viale Andrea Doria 6, 95125 Catania, Italy. E-mail: antonino.gulino@unict.it*

[b] *CNR-IMM, Z.I. VIII Strada 5, Catania, 95121, Italy*

[c] *Department of Engineering, University of Messina, Contrada Di Dio, 98166 Messina, Italy.*

[d] *Chemical Research Support, Weizmann Institute of Science, Rehovot 7610001, Israel.*

[e] *Department of Molecular Chemistry and Materials Science, Weizmann Institute of Science, Rehovot 7610001, Israel.*

Table S1. Preliminary synthesis investigations to optimize the reaction method and conditions.

Solid state syntheses

Mo source	S source	Temperature °C	Reaction time / h	Main product
$MoO_2(acac)_2$	Sublimed S	350	24	MoO_3
$MoO_2(acac)_2$	Na_2S	350	24	MoO_3
$MoO_2(acac)_2$	Molar excess of sublimed S	350	24	MoO_3

Solvothermal syntheses

Mo source	S source	Solvent	pH	Temperature °C	Reaction time / h	Main product
Na_2MoO_4	CH_3CSNH_2	H_2O	HCl 4M	100	24	MoS_2 /

						MoO_3
Na_2MoO_4	CH_3CSNH_2	H_2O	neutral	200	24	MoS_2 / MoO_3
$MoO_2(acac)_2$	Sublimed S	NMP		180	24	Low yield
$MoO_2(acac)_2$	Sublimed S	NMP		200	24	MoS_2/C composite
$MoO_2(acac)_2$	Sublimed S	NMP		220	24	Low yield
MOCVD						
$MoO_2(acac)_2$ / g	Sublimed S/g	Ar flux / sccm	Substrate	Substr Temp / °C	Pressure / Torr	Main product
0,2065	0,0389 (molar S/Mo= 2)	500	Si	800	5	Negligible MoO_3
0,2022	0,6224 (molar S/Mo=32)	350	Si	800	5	Negligible MoO_3
0,1006	0,4923(molar S/Mo=51)	350	Si, SiO_2	750	5	Negligible MoO_3
0,1105	0,4929 (molar S/Mo= 51)	50 (in the reactor) 150 (carrier gas)	Si, SiO_2	500	5	Negligible MoO_3
0,1105	0,4929 (molar S/Mo= 51)	100 (in the reactor) 150 (carrier gas)	MoO_3	700	5	Negligible MoO_3

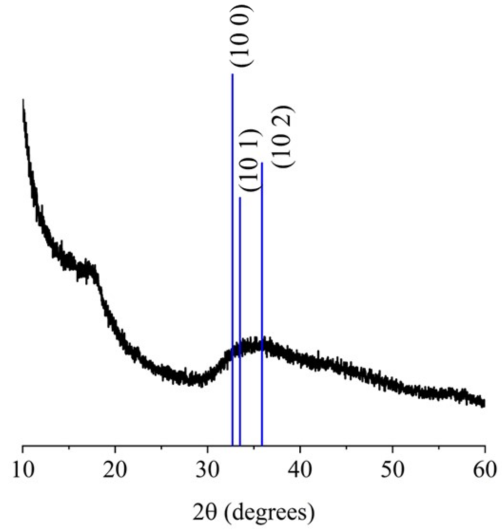

Fig. S1. XRD pattern of the MoS_2/C composite.The superimposed blue lines denote the position of the most intense reflections expected for the hexagonal MoS_2 phase (PDF Card No: 065-0160).

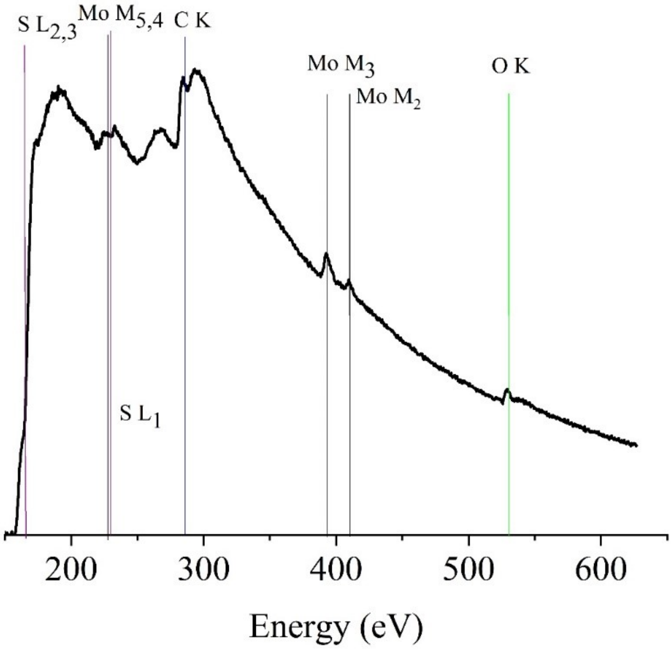

Fig. S2 EELS spectrum of the MoS_2/C composite showing the S L-edge, Mo M-edge, C K-edge, and the O K-edge peaks. The peaks are evident for the S $L_{2,3}$- and L_1-edges at 165 and 229 eV, respectively; Mo $M_{5,4}$-,M_3-, and M_2-edges at 227, 392, and 410 eV, respectively; the C K-edge at 284 eV and the O K-edge at 532 eV. Specifically, for the C K-edge, the transitions that involve the π* and σ* orbitals are evident, indicating a sp²-hybridized carbon, thus confirming the graphitic nature of the carbon matrix.[49]

The electrochemical properties of the SPCE and MoS_2/C composite /SPCE sensors were studied by CV using a scan rate of 50 mV/s (Figure S3a). We noticed that the MoS_2/C composite SPCE sensor shows a CV cycle involving a larger current variation (4.38 μA at 0.6 V) than that of the SPCE sensor (0.23 μA at 0.6 V), which can also be attributed to the larger surface area present on this electrode.[1] The CV (Figure S3b), conducted in the presence of the reversible redox standard probe $K_3[Fe(CN)_6]$, shows more intense anodic and cathodic peak currents for the MoS_2/C composite /SPCE sensor than those observed for the SPCE sensor, thus demonstrating a better sensitivity, with a fully reversible trend. Furthermore, the difference between the anodic and cathodic peaks is characterized by a significant decrease in the volatile potential, ranging from 291 mV for the bare SPCE to 148 mV for MoS_2/SPCE. This trend shows the better ability of the modified sensor to transfer charges, thus favoring the redox reaction and confirming that the MoS_2-modified electrode shows improved electrochemical capabilities.[2]

The EIS analysis of the MoS_2/SPCE sensor reveals an almost linear behavior of the resistance (the real part of impedance) *versus* the reactance (the imaginary part of impedance), thus highlighting the good electron transfer properties of the MoS_2/SPCE sensor and the mechanism governed by the diffusion (Figure S3c, inset equivalent circuit).[2-4] This behavior was confirmed by the CV measurements conducted at different scan rates (from 25 to 400 mV/s) (Figure S3d). Specifically, the anodic peak current increases linearly with the square root of the scan rate, thus confirming that the electrochemical redox reaction is controlled by a diffusion process.[2]

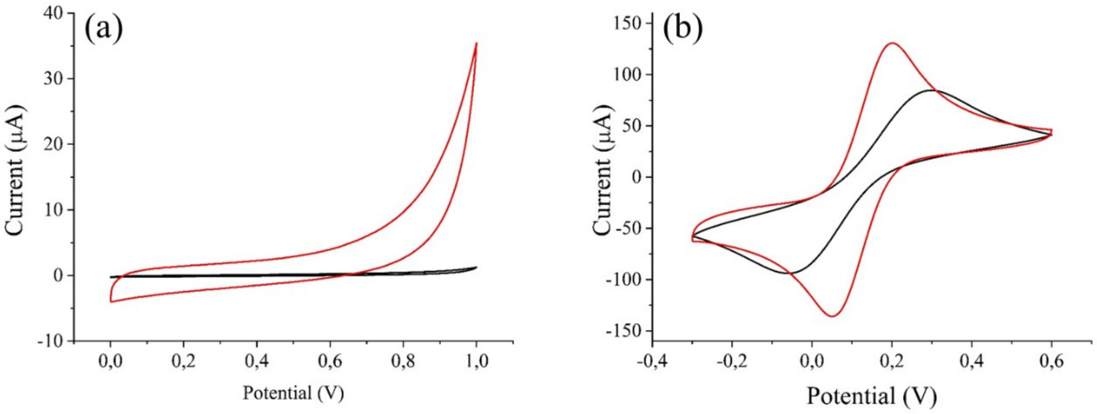

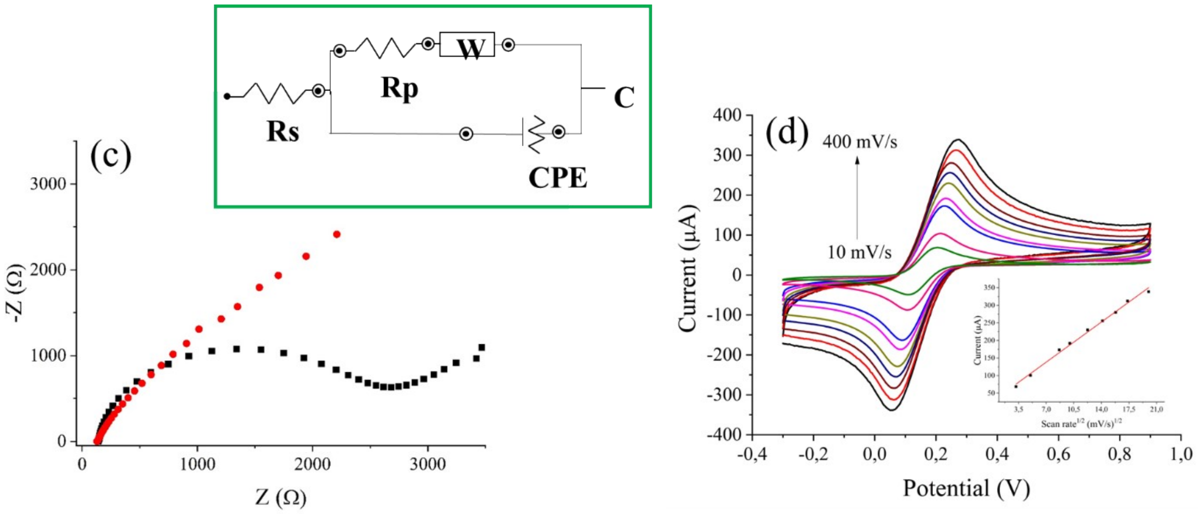

Fig. S3 (a) Electrochemical behavior of SPCE in 0.1 M PBS at a scan rate of 50 mV/s (the black line), MoS_2/SPCE (the red line), in the 0.0–1.0 V potential window; (b) Cyclic voltammogram of SPCE (black line), MoS_2/SPCE (the red line) in the presence of 10 mM $K_3[Fe(CN)_6]$ and at a 50 mV/s scan rate, in the -0.3–0.6 V potential window. (c) EIS of SPCE (the black squares) and MoS_2/SPCE (the red dots) with the equivalent circuit in the inset; (d) Cyclic voltammogram of MoS_2/SPCE in the presence of 10 mM $K_3[Fe(CN)_6]$ at different scan rates ranging from 25 to 400 mV/s in 0.1 M PBS (pH 7.4), (inset) Plot of Ip *vs* $\upsilon^{1/2}$.

Electroanalytical analyses were conducted on the MoS_2/SPCE sensor to assess its ability to detect the nitrite (NO_2^-) anion; Figure S4a shows the LSV response for a 200 μM nitrite anion in 0.1 M PBS.[1,2] The MoS_2/SPCE sensor has better ability than that of the bare SPCE to detect this analyte; the current peak intensity value (I_p) is more than twice as high for MoS_2/SPCE than for SPCE (Figure S4b). Given the modified sensor's improved ability to catalyze the nitrite oxidation reaction, we investigated the ability of MoS_2/SPCE to detect different concentrations of nitrite ions through LSV and DPV analyses. The experimental LSV results, reported in Figure S5a, show that the current increases with the increase in the nitrite ion concentration (in the 0-1000 μM range, with initial steps of 10 μM), thus highlighting the excellent ability of MoS_2/SPCE to detect different NO_2^- concentrations (LOD = 2 μM; the calibration curve is shown in Figure S5b).

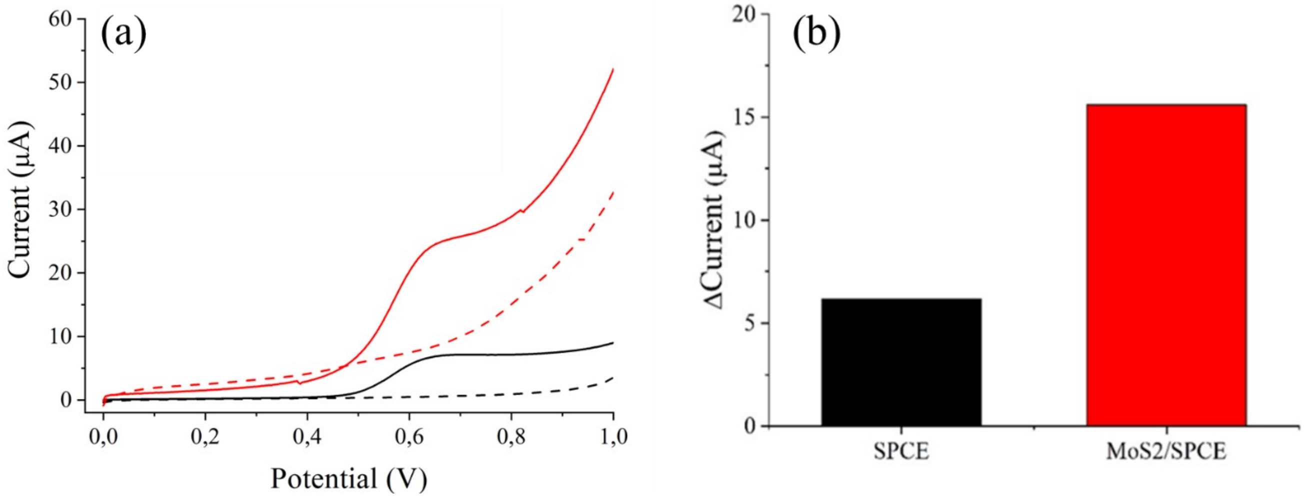

Fig. S4 (a) Electrochemical behavior of SPCE (0-1 V potential range) in PBS (the black dotted line) and MoS_2/SPCE (the red dotted line) and in the presence of 200 μM of $NaNO_2$ of SPCE (the black solid line) and MoS_2/SPCE (the red solid line); (b) comparison between the responses of SPCE and MoS_2/SPCE in the presence of 200 μM of $NaNO_2$.

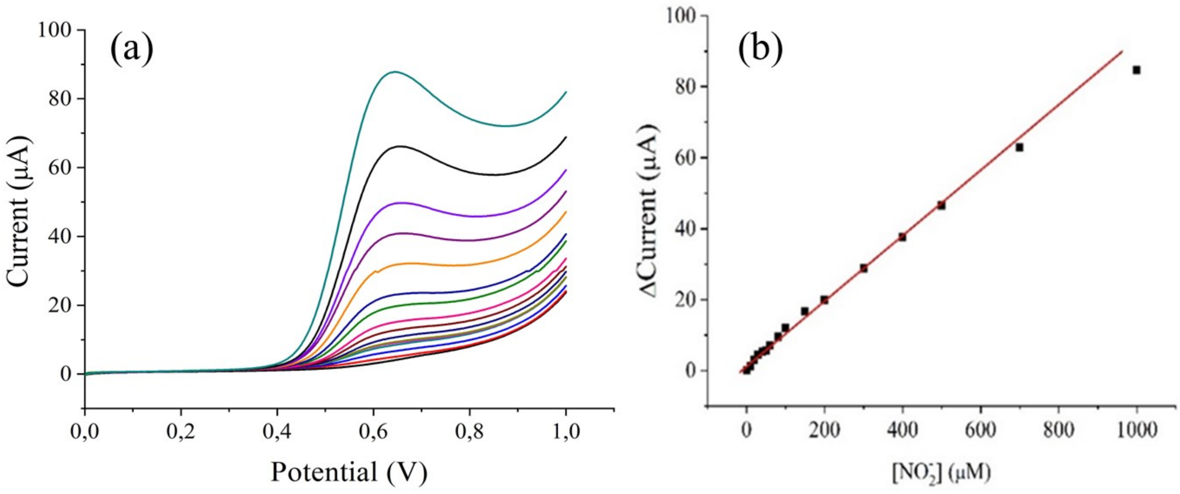

Fig. S5 (a) LSV of MoS_2/SPCE at different nitrite concentrations (0-1000 μM, in initial steps of 10 μM) in the presence of 0.1 M PBS (pH 7.4) and at a scan rate of 50 mV/s; (b) graph of the anodic peak current (I_{pa}) *versus* the NO_2^- concentration. The I_{pa} values were obtained from LSV performed with MoS_2/SPCE for solutions with different concentrations of $NaNO_2$.

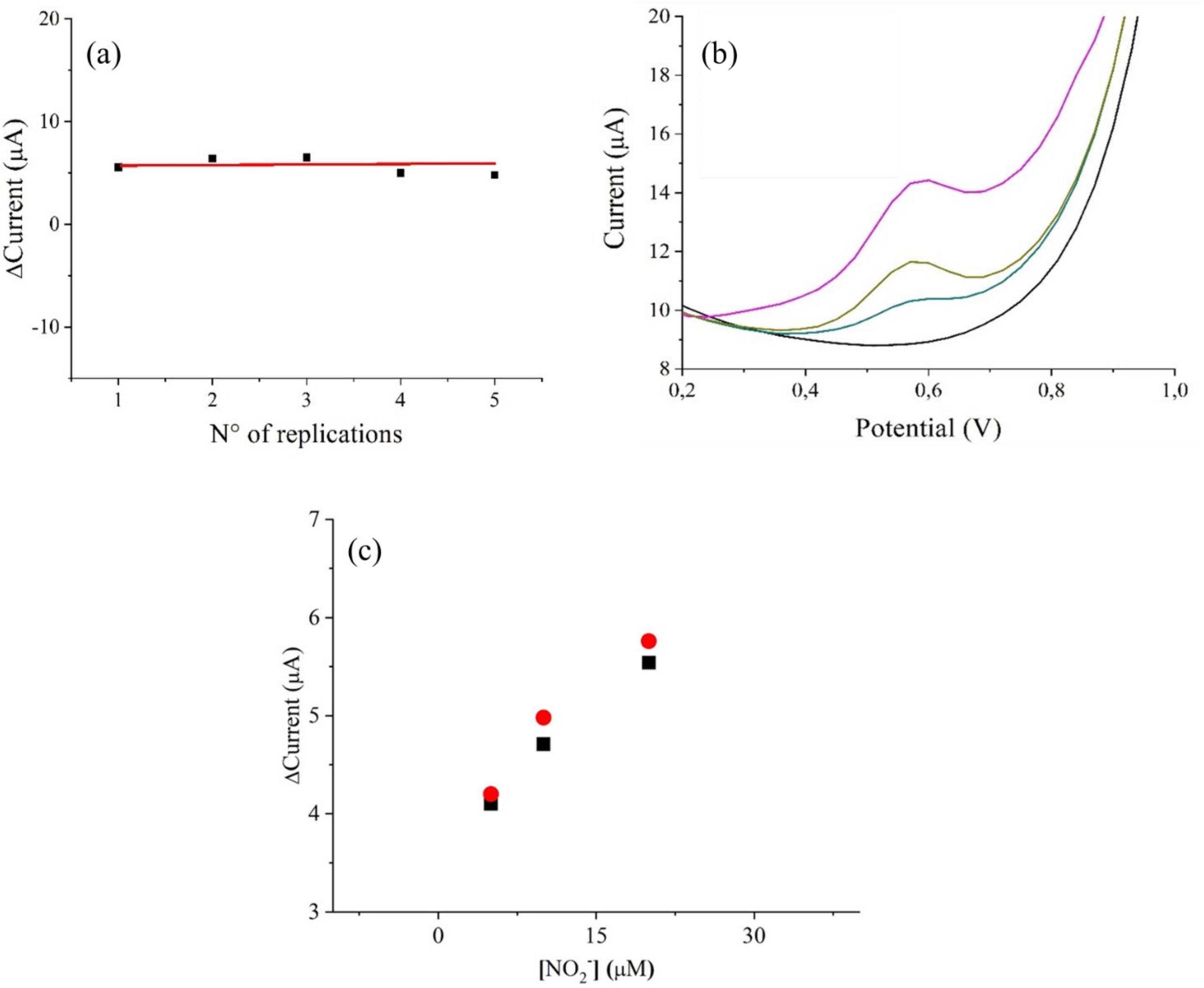

Fig. S6 (a) Repeatability of the detection of $NaNO_2$ (20 *m*M) with an MoS_2/SPCE of (SD = 0.78 for 5 repeated whole cycles). (b) DPV analyses to determine 1 (dark cyan), 2 (dark yellow), and 20 (magenta) μM of $NaNO_2$, added to the real water sample (Fontenoce; the black line). (c) DPV analyses showing the response of MoS_2/SPCE to 5, 10, and 20 μM of $NaNO_2$ at *t* = 0 (the black squares) and at t = 6 months (the red dots).

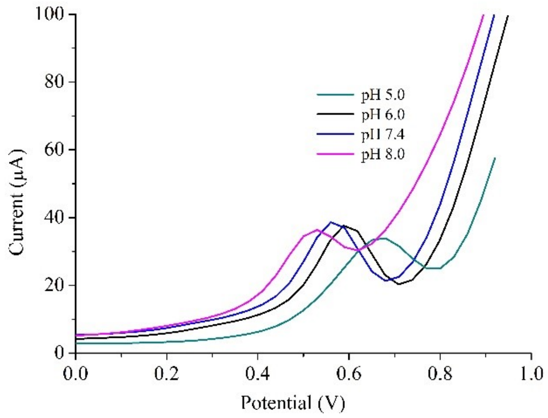

Fig. S7 DPV analyses showing the response of MoS_2/SPCE to 200 μM of $NaNO_2$ a different pH values (5.0, 6.0, 7.4, 8.0).

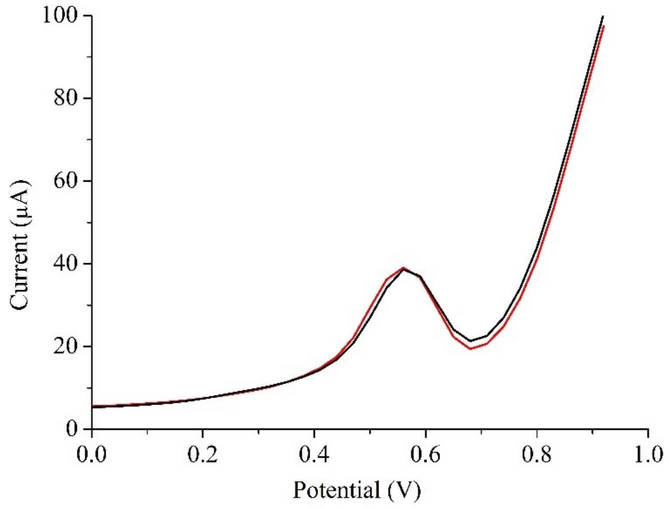

Fig.S8 DPV analyses showing the response of MoS_2/SPCE to 200 μM of $NaNO_2$ in PBS 0.1 M (black line), and PBS 0.1 M and NaCl 0.1 M (red line)

References

1. A. Ferlazzo, C. Espro, D. Iannazzo, A. Bonavita and G. Neri, *Mater. Today Commun.,* 2023, **35**, 106036.
2. R. Zribi, A. Ferlazzo, E. Fazio, M. Condorelli, L. D'Urso, G. Neri, C. Corsaro, F. Neri, G. Compagnini and G. Neri, *IEEE Trans. Instrum. Meas.,* 2023, **72**, 1–8.
3. A. Ferlazzo, C. Celesti, D. Iannazzo, C. Ampelli, D. Giusi, V., Costantino, and G. Neri, *ACS Omega*, 2024, **9**, 27085–27092.
4. H. L. Zou, L. Y. Qin, H. Q. Luo, B. L. Li and N. B. Li, *Sens. Actuator B-Chem.,* 2021, **337**, 129812.